



CHORUS

This is the accepted manuscript made available via CHORUS. The article has been published as:

Radiolysis to knock-on damage transition in zeolites under electron beam irradiation

O. Ugurlu, J. Haus, A. A. Gunawan, M. G. Thomas, S. Maheshwari, M. Tsapatsis, and K. A. Mkhoyan

Phys. Rev. B **83**, 113408 — Published 29 March 2011

DOI: [10.1103/PhysRevB.83.113408](https://doi.org/10.1103/PhysRevB.83.113408)

Radiolysis to Knock-on Damage Transition in Zeolites Under Electron Beam Irradiation

O. Ugurlu¹, J. Haus², A.A. Gunawan², M.G. Thomas³, S. Maheshwari², M. Tsapatsis² and, K.A. Mkhoyan^{2*}

¹*Characterization Facility, University of Minnesota, Minneapolis, Minnesota 55455*

²*Department of Chemical Engineering and Materials Science,
University of Minnesota, Minneapolis, Minnesota 55455*

³*Cornell Center for Materials Research, Cornell University, Ithaca, New York 14853*

The electron beam induced damage in a zeolite under 60 to 200 keV energy beam irradiation has both radiolytic and knock-on components and can be described by linear superposition of these two processes. Theoretical predictions supported by experiments at 60 keV suggest that for electron beam energies smaller than 70 keV the damage of specimen follows through a radiolytic path. For energies larger than 200 keV knock-on based sputtering of material will dominate, while considerable radiolytic movement of the atoms will still be present.

Elastic and inelastic scattering of energetic electrons in specimens are essential for imaging and spectroscopy in transmission electron microscopy (TEM). They are also responsible for electron-beam-induced alterations of specimens limiting quantitative analysis. The most common damage mechanisms can be classified under knock-on damage and radiolysis^{1,2}. Every sample is subject to knock-on damage if the energy of incident electrons is high enough to overcome the threshold energy of atomic sputtering^{3,4}. Radiolysis, on the other hand, introduces atomic displacements in a solid by converting excitonic energies generated during incident-probe/atomic-electron interactions into momentum by forming a Frankel pair⁵. For radiolysis, the energy stored in exciton should be as large as the energy necessary for atomic displacement and the relaxation time for the exciton should be long enough ($\gtrsim 1$ ps) so that mechanical relaxation of the atoms can lead to bonding instabilities. As a result, induced atomic displacement is primarily observed in ice, organics, halides and silicates¹.

While it is expected that many materials should be susceptible to both types of electron beam damage at high electron energies ($\gtrsim 100$ keV), there is no such reported case. The occurring damage is found to be either radiolytic or knock-on. Silicate-based material have shown to be altered by either damage mechanisms: Hobbs *et al.*⁶ and Ihui *et al.*⁷ reported radiolysis driven crystalline-to-amorphous transformation in α -quartz, while Chen *et al.*⁸ measured mass-loss in amorphous-SiO₂ due to knock-on damage. This raises a question of whether these two mechanisms can be considered independent and the dominance of one is due to difference in damage rates, *or*, presence of one mechanism fundamentally affects the other, for example, presence of knock-on scatterings changes the excitonic states critical for radiolysis.

In this Letter, we show that in a case of a certain zeolite, for wide range of incident electron energies both knock-on and radiolytic electron-beam damage mechanisms are active and linear superposition of these two processes, characteristic for independent processes, can be used to evaluate the total rate of the damage. Experimental high-resolution imaging and electron energy loss spectroscopy (EELS) studies presented here and a comparison with theoretical damage cross-sections indicate that when electron beam energy is smaller than 70 keV only radiolysis is active and when it is larger than 70 keV both mechanisms contribute. These results are of particular significance because understanding of electron beam damage in zeolites^{9–12} could improve their structure identification^{13–15}.

The aluminosilicate zeolite MCM-22 (framework type MWW¹⁶) formed by calcination of a layered precursor¹⁷, MCM-22(P), with 2.5 nm thick layers and a Si/Al ratio of 46.7 has been used in this study. Electron transparent samples were prepared by sonication of small particles for about 5 minutes in isopropanol that were picked up by a standard holey-carbon TEM grid. The experiments were carried out in two different TEMs: FEI Tecnai G2 F-30 300kV scanning and transmission electron microscope ((S)TEM) equipped with a Schottky field emission gun, S-twin lens, Gatan Enfina-1000 energy loss spectrometer and low-angle and high-angle annular dark field (ADF) detectors, and Nion aberration-corrected dedicated Ultra-STEM¹⁸.

During knock-on damage an incident energetic electron of the probe in a direct collision transfers a significant amount of energy to the atoms of the specimen, which can be sufficient to remove an atom from its site or sputter it from the surface^{19,20}. The maximum energy that can be transferred to an atom in a collision is^{3,4}:

$$E_{max} = \frac{2E(E + 2m_0c^2)}{M_0c^2}, \quad (1)$$

where E is the energy of incident electrons, M_0 is the mass of the atom, and $m_0c^2 = 511$ keV is the rest energy of the electron. This equation also provides the threshold energy, $E_{th}^{(1)}$, that incident electrons must have to be able to displace or sputter atoms from a site in a solid. The probabilities for vacancy-enhanced displacement and surface sputtering, which are the two dominating processes for knock-on damage, can be described using the Mott cross-sections^{3,21}. The Mott cross-section for surface sputtering (which is the limiting mechanism) for relativistic incident electron can be expressed as^{4,22}:

$$\sigma_k(E) = \pi \left(\frac{Ze^2}{m_0c^2} \right)^2 \frac{1 - \beta^2}{\beta^4} \times \left[(\xi - 1) - \beta^2 \ln(\xi) + \pi\alpha\beta \left\{ 2 \left[\xi^{\frac{1}{2}} - 1 \right] - \ln(\xi) \right\} \right], \quad (2)$$

where Z is the atomic number, $\alpha = Z/137$, $\xi = E_{max}/E_{th}^{(1)}$ and $\beta = v/c = \sqrt{1 - (1 + E/m_0c^2)^{-2}}$. The Si-O binding energy in silicates is about 5-5.5 eV/bond²³ resulting in the threshold energies for oxygen and silicon atoms in the zeolite to be about 70 and 115 eV, respectively. Dependence of the cross-sections of knock-on damage on incident electron energy for oxygen and silicon atoms are presented in Fig. 1, where $\sigma_k(E)$ has non-zero value at energies $E > E_{th}^{(1)}$. This suggests that in microscopes with beam energy lower than 65 keV knock-on damage should not occur. Since the fraction of Al in the sample is small, its presence is neglected in the modelled structure.

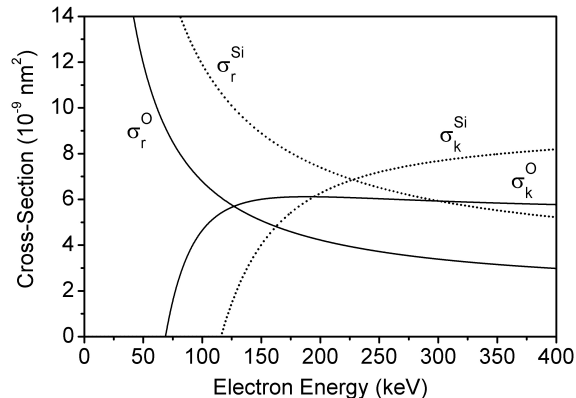


FIG. 1. Calculated cross-sections for radiolytic movement and knock-on surface sputtering for silicon and oxygen atoms in the MCM-22 zeolite as a function of incident electron energy.

The cross-section of radiolytic movement of atoms in a specimen for relativistic incident electron is given as¹:

$$\sigma_r(E) = \pi \left(\frac{Ze^2}{m_0c^2} \right) \frac{2e^2}{E_{th}^{(2)}\beta^2} \times \zeta, \quad (3)$$

where $E_{th}^{(2)}$ is the threshold energy that must be transferred to the electrons of the atom to produce atomic movement. It is defined by bond strength and coordination number of the atom within the specimen. The efficiency factor ζ in Eq. (3) in silicates is $\zeta \simeq 10^{-41}$. The calculated cross-sections for the radiolytic movement of silicon and oxygen atoms in the zeolite are presented in Fig. 1.

A series of conventional high-resolution bright-field TEM images of MCM-22 zeolite were collected using FEI-(S)TEM. They were recorded with 5 second intervals at four accelerating voltages: 60, 80, 100, and 200 kV. The electron beam current, measured using the drift tube of the EELS with the magnet switched off, was 0.14 nA during acquisition of all the images. To avoid the effects of specimen thickness on the damage rate, data from samples with similar thicknesses were selected for further analysis. The thickness of each sample was measured using the ratios of the intensities of the single plasmon-loss to the zero-loss: $t = [I_{pl}/I_0] \cdot \lambda_{pl} = 0.07\lambda_{pl}$, where λ_{pl} is the mean-free-path of plasmon generation^{24,25}. The estimated thickness was about 7.5 ± 1 nm.

Fast fourier transforms (FFT) of the high resolution images were calculated to evaluate electron-beam-induced damage. Intensity of the spots, I_c , corresponding to periodic fringes in the image and the rings, I_a , corresponding to amorphous layer were obtained from the FFT of each image. (see Fig. 2(a-f)). To estimate the damage rates, the ratio $R = (I_c - I_a)/I_a$, which represents degradation of the crystal structure of the sample from crystalline to amorphous was evaluated²⁶. Then, the slope of the linear fit to the data set of decaying ratio, R , as a function of time was used as a damage rate (see inset in Fig. 2(f)). The summary of damage rates obtained for incident beams with 60, 80, 100, and 200 keV energy electrons are presented in Fig. 3. For comparison with theoretical predictions, the data was fitted to the total damage cross-section function combining both knock-on and radiolytic scattering processes, $f(E) = A\sigma_{Total}^{Si-O}(E) = A[\sigma_k^{ave}(E) + \sigma_r^{ave}(E)]$. A single fitting parameter, A , incorporates the incident beam current density and the crystal-to-amorphous transition factor. Average for $[\text{SiO}_2]$ unit cross-sections were used for the sample. The remarkable correlation of the theory and experiment on damage behaviour suggests that indeed both damage mechanisms are present during degradation of the zeolite sample when it is exposed to electron beam with an energy larger than 70 keV.

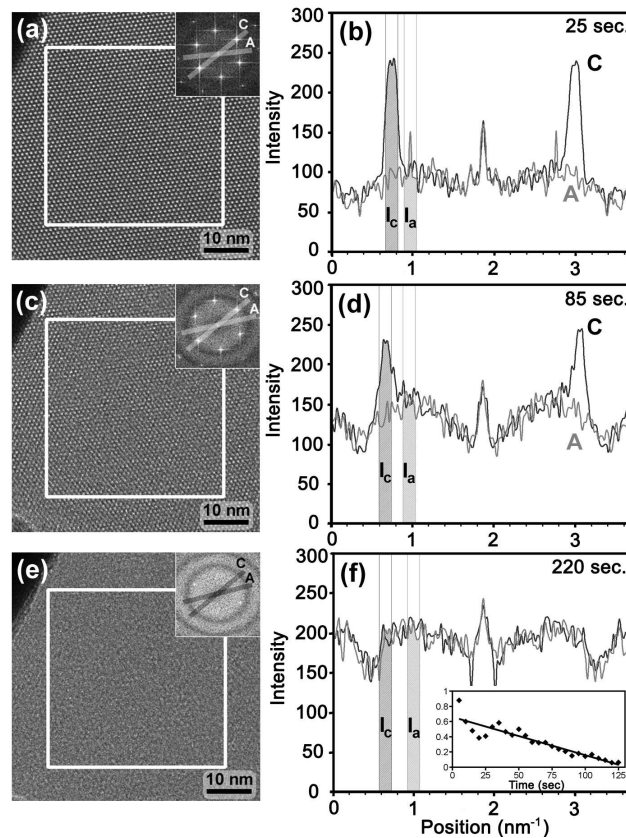


FIG. 2. (a) High-resolution TEM image of MCM-22 zeolite recorded after 25 seconds of 200 keV electron beam exposure. The inset at top-right corner is FFT obtained from highlighted area in the image. (b) Two line-scans from the FFT shown in (a) labelled 'A' and 'C'. (c-d) Same area of the sample after 85 seconds of beam exposure. (e-f) The area after 220 seconds of beam exposure. The inset in (f) is evaluation of the ratio $R = (I_c - I_a) / I_a$ as a function of exposure time with linear fit.

To confirm these observations, EELS measurements were conducted under the same conditions as imaging with 200 keV electron beam. EELS spectra of Si $L_{2,3}$ - and O K -edges were recorded simultaneously with 10 second intervals and 4 seconds acquisition time from a 5×10^3 nm² area of the sample as crystal structure of the specimen was degrading under electron beam exposure. Integrated intensity of both Si $L_{2,3}$ - and O K -edges were calculated after standard background subtraction^{20,24} and plotted as a function of beam exposure time (Fig. 4). Strong reduction of the number of Si and O atoms from the exposed area is an indication that considerable knock-on-based sputtering of the material is taking place at 200 keV, which is consistent with theoretical predictions (see Fig. 1 and 3).

For damage with 60 keV electrons, Nion aberration-corrected STEM was used to irradiate the samples and record ADF images. Fig. 5(a) and (b) shows high-resolution ADF images of a layer of MCM-22 zeolite (c-axis of the sample was oriented parallel to incident beam) before and after beam damage. While the loss of crystal structure is apparent, it is not clear that mass-loss has taken place. The ADF intensity, I_{adf} , which is proportional to the number of atoms in the exposed area and the average atomic number (Z) of the sample²⁷, was calculated before and after beam damage. The ratio of the ADF intensities obtained from entire images, $I_{adf}^{before} / I_{adf}^{after} = 0.99$, indicates that atomic sputtering is not an active scattering process, therefore, confirming that radiolysis is the damage mechanism at 60 keV.

To estimate the range of atomic movements in zeolites initiated by radiolysis, the STEM probe was held at one point on the sample for about 10 seconds to form a hole. A low magnification ADF image of the area was taken right after (see Fig. 5(c)). Increased intensity in ADF image in areas around the edges of the hole is due to accumulation of additional material from the irradiated 'hole' area. A line-scan obtained from the image across the hole is compared with a similar line-scan obtained from the non-irradiated nearby area and the results are shown in Fig. 5(c) and (d). It can be seen that radiolysis in this zeolite produces about 2-3 nm mass displacement.

In conclusion, we observed that electron beam induced damage in zeolite at moderate 60 to 200 keV electron energy range, typical for most TEMs, has both radiolytic and knock-on components and can be described by linear superposition of these two processes typical for independent processes. Experimental observations supported by theoretical predictions, based on scattering cross-sections, suggest that for the electron beam energies smaller than

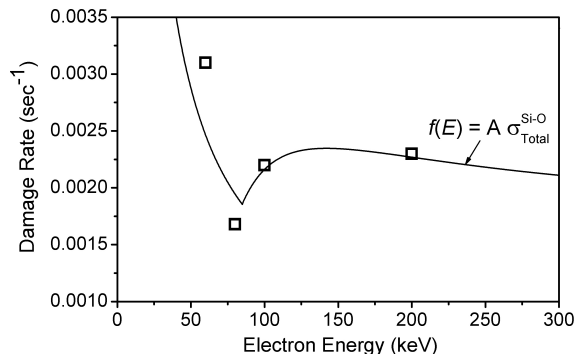


FIG. 3. Comparison of the measured degradation rate in MCM-22 zeolite with calculated total cross-section, $\sigma_{Total}^{Si-O}(E)$, that includes both radiolysis and knock-on damage mechanisms.

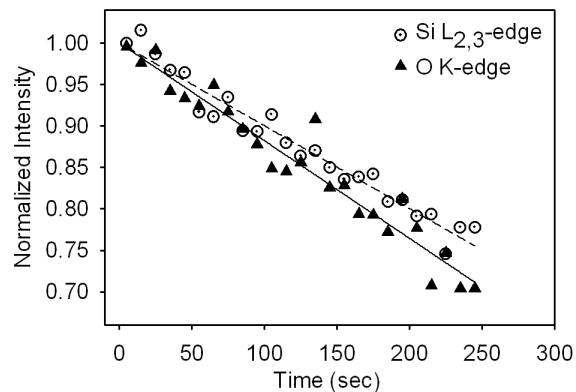


FIG. 4. Measured integrated intensity of the Si $L_{2,3}$ - and O K -edge EELS spectra as a function of beam exposure time. Starting from edge onset 20 eV energy range was used for integration and the results were normalized to initial spectrum. 200 keV electron beam was used here.

70 keV the damage follows through only radiolytic path. However, for energies bigger than 200 keV, knock-on based spattering of material from the surface is expected to be dominant, while considerable radiolytic movement of the atoms will still be present. It was also observed that during radiolysis mass displacement is about 2-3 nm. The results also suggest that operating the TEM with 80 keV electron beam will minimize the beam damage in similar zeolites. These results also suggest that both radiolytic and knock-on damage mechanisms should be present in many silicates, including different crystalline or amorphous forms of SiO_2 sharing similar ($\sim 5\text{eV}$) atomic bonding energies. We believe that lack of analytical capabilities in early TEMs prevented Hobbs *et al.*⁶, Ihui *et al.*⁷ and Chen *et al.*⁸ to detect both damage mechanism.

This work was supported partially by the NSF MRSEC program DMR-0819885. This work utilized the University of Minnesota Characterization Facility, with partial support from the NSF-NNIN and the NSF MRSEC programs and, the Advanced Electron Microscopy facility of the Cornell Center for Materials Research with support from the

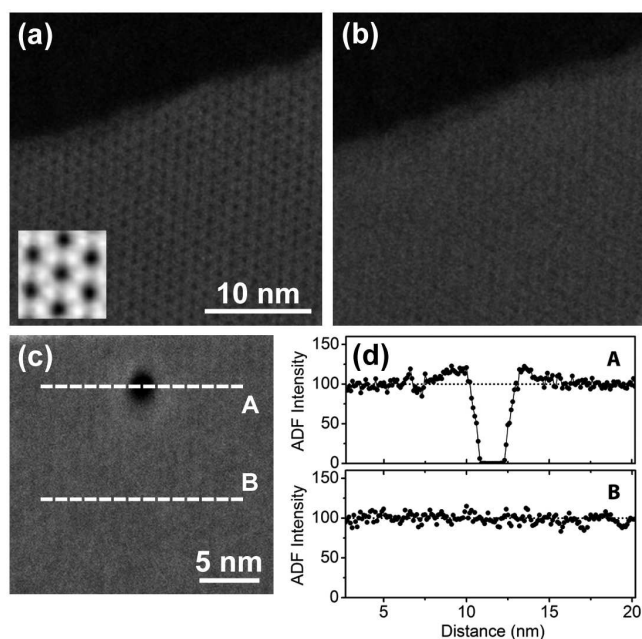


FIG. 5. High-resolution ADF-STEM image of MCM-22 zeolite recorded using 60 keV aberration-corrected STEM before the damage. The inset at bottom-corner is a portion of the same image after statistical improvement. (b) Sample in (a) after 35 seconds of beam exposure with 40 pA beam current. (c) ADF image of another area after hole formation under intensive point beam. (d) Two line-scans from image in (c).

NSF MRSEC program DMR-0520404.

-
- ¹ L.W. Hobbs, *Introduction to Analytical Electron Microscopy*, J.J. Hren, J.I. Goldstein, D.C. Joy, Editors. 1979, p. 437; *Scanning Microscopy Supplement 4*, J. Schou, P. Kruit, D.E. Newbury, Editors. 1990, p. 171.
 - ² L. Reimer and H. Kohl, *Transmission Electron Microscopy: Physics of Image Formation, 5th edition* (Springer, Berlin 2008).
 - ³ N.F. Mott, Proc. R. Soc. London, Ser A **135**, 429 (1932).
 - ⁴ C.R. Bradley, *Calculations of Atomic Sputtering and Displacement Cross-Sections in Solid Elements by Electrons with Energies from Threshold to 1.5 MeV*, Report No. ANL-88-48, 1988.
 - ⁵ M.N. Kabler and R.T. Williams, Phys. Rev. B **18**, 1948 (1978)
 - ⁶ L.W. Hobbs and M.R. Pascucci, J. de Physique **41**, 237 (1980); M.R. Pascucci, J.L. Hutchison, and L.W. Hobbs, Radiation Effects **74**, 219 (1983).
 - ⁷ H. Inui, H. Mori, T. Sakata and H. Fujita, J. Non-Cryst. Solids **116**, 1 (1990).
 - ⁸ G.S. Chen, C.B. Boothroyd, and C.J. Humphreys, Phil. Mag. A **78**, 491 (1998).
 - ⁹ R. Csencsits and R. Gronsky, Zeolites **8**, 122 (1988).
 - ¹⁰ M.M.J. Treacy and J.M. Newsam, Ultramicroscopy **23**, 411 (1987).
 - ¹¹ L.A. Bursill, E.A. Lodge, and J.M. Thomas, Nature **286**, 111 (1980).
 - ¹² Y. Yokota, H. Hashimoto, and T. Yamaguchi, Ultramicroscopy **54**, 207 (1994).
 - ¹³ F. Gramm, C. Baerlocher, L.B. McCusker, S.J. Warrender, P.A. Wright, B.Han, S.B. Hong, Z. Liu, T. Ohsuna, and O. Terasaki, Nature **444**, 79 (2006).
 - ¹⁴ J. Ruan, P. Wu, B. Slater, and O. Terasaki, Angew. Chem. Int. Ed. **44**, 6719 (2005).
 - ¹⁵ P. Wu, J. Ruan, L. Wang, L. Wu, Y. Wang, Y. Liu, W. Fan, M. He, O. Terasaki, and T. Tatsumi, J. Am. Chem. Soc. **130**, 8178 (2008).
 - ¹⁶ Ch. Baerlocher, L.B. McCusker, D.H. Olson, *Atlas of Zeolite Framework Types* (Elsevier, 2007).

- ¹⁷ M.E. Leonowicz, J.A. Lawton, S.L. Lawton, M.K. Rubin, *Science* **264**, 1910 (1994).
- ¹⁸ D.A. Muller, L.F. Kourkoutis, M. Murfitt, J.H. Song, H.Y. Hwang, J. Silcox, N. Dellby, and O. L. Krivanek, *Science* **319**, 1073 (2008).
- ¹⁹ D.L. Medlin, L.E. Thomas and D.G. Howitt, *Ultramicroscopy* **29**, 228 (1989).
- ²⁰ K.A. Mkhoyan and J. Silcox, *Appl. Phys. Lett.* **82**, 859 (2003).
- ²¹ H. Feshbach, *Phys. Rev.* **103**, 1597 (1956).
- ²² W.A. McKinley and H. Feshbach, *Phys. Rev.* **74**, 1759 (1948).
- ²³ D.M. Teter, G.V. Gibbs, M.B. Boisen, D.C. Allen, M.P. Teter, *Phys. Rev. B* **52**, 8064 (1995).
- ²⁴ R. Egerton, *Electron Energy Loss Spectroscopy in the Electron Microscope* (Plenum, New York, 1996).
- ²⁵ K.A. Mkhoyan, T. Babinec, S.E. Maccagnano, E.J. Kirkland and J. Silcox, *Ultramicroscopy* **107**, 345 (2007).
- ²⁶ The analysis is limited by inherent difference between actual fractions of crystalline and amorphous portions of the specimen and their visibility in high-resolution TEM images, which can be 20%.
- ²⁷ S.J. Pennycook and L.A. Boatner, *Nature* **336**, 565 (1988); S.J. Pennycook and D.E. Jesson, *Ultramicroscopy* **37**, 14 (1991).